

Study for plasma etching of dielectric film in semiconductor device manufacturing. Review of ASET research project*

Makoto Sekine

Plasma Technology Laboratory, Association of Super-advanced Electronics Technologies (ASET), 292 Yoshida, Yokohama 244-0817, Japan

Abstract: Conventional developments were conducted in a very empirical way, such as a trial and error with many speculations using qualitative data. This approach requires more and more resources and time for the development of future devices with a design rule below 100 nm in the system on a chip (SOC) era. It is necessary to establish a systematic methodology for process development and qualification. ASET Plasma Laboratory had been found to research a basis for the systematic development of the plasma etching technology. Fluorocarbon (CF) plasma for the etching of high-aspect-ratio contact holes in SiO₂ was investigated intensively in the 5-year program that finished in March 2001. They introduced 5 plasma sources that can etch 0.1- μ m contact holes on a 200-mm wafer in production, and state-of-the-art diagnostics tools for the plasma and etched surface. The SiO₂ etch mechanism was revealed from the etch species generation to the reaction in a deep hole. The number of electron collisions to fluorocarbon gas molecule is proposed as an important parameter to control the gas dissociation and etch species flux to the surface. An etch reaction model was also proposed using the estimated-surface-reaction probability that is a function of ion energy and CF polymer thickness that reduces the net ion energy to the reaction layer. The CF polymer thickness was determined by a balance equation of generation term (radical fluxes) and loss terms (etching by ions, radicals, and out-flux oxygen from SiO₂). A program was developed and successfully predicts the etch rates of Si-containing materials, including organic dielectrics. Requirements for the next-generation plasma etch tools are also discussed.

INTRODUCTION

High-density plasma (HDP) sources were developed well for the etching of metals and gate materials, but failed in the SiO₂ etching, because of low controllability for the complicated chemistry of the oxide etching. On the other hand, the capacitively coupled (parallel plate) plasma sources that have been improved, become the standard for the SiO₂ etching nowadays. However, the prospects of future device manufacturing urge us to resolve technology barriers fast. Conventional development with an empirical and speculative approach requires tremendous resources and time for the near future devices with a design rule below 100 nm in the system on a chip (SOC) era. It is necessary to establish a systematic methodology for process development and qualification.

ASET is a Japanese electronics research and development consortium founded in February 1996. The Plasma Technology Laboratory has accomplished a 5-year project to understand the reactive

*Lecture presented at the 15th International Symposium on Plasma Chemistry, Orléans, France, 9–13 July 2001. Other presentations are presented in this issue, pp. 317–492.

plasma processing scientifically and quantitatively for establishing a basic footing technology to control the plasma processing and exploit the etch systems effectively [1]. We chose an etching technology for forming fine contact holes less than 100 nm in diameter to SiO₂ film over Si using fluorocarbon (CF) gas plasma as a subject. SiO₂ film is a very common dielectric material used in all Si-based LSI devices for a long time. CF plasma achieves high performance, such as high selectivity to Si and photoresist, however, its reactions in the gas phase and surface are so complicated that it is very difficult to analyze quantitatively and understand. Once the mechanism and control methodology is accomplished in CF plasma, its impact on technology development, including the etching of other materials, is extensive. In this review, the results of the ASET project and issues of the etch technology will be reviewed.

RESEARCH SYSTEM

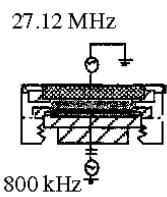
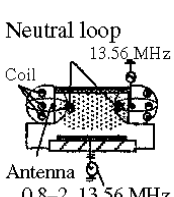
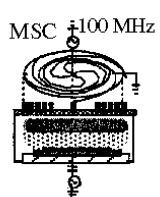
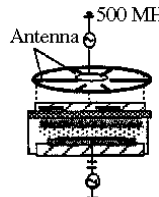
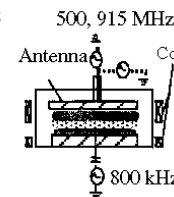
In the first half of the project, while introducing five etching reactors that achieve production-worthy processing with $\Phi = 200$ -mm wafer, state-of-the-art diagnostics systems were installed for *in situ* measuring of the gas-phase parameters and radicals. In the second half, we began research on surface reactions. Phenomena in high-aspect-ratio holes were also investigated. Based on our understanding of the key parameters in etching reactions, some monitoring tools and a simulation were proposed to control and predict the etching process.

Table 1 describes the five etch reactors [2–6]. These tools each have specific processes that can form SiO₂ contact holes less than 200 nm in diameter, the aspect ratio (hole depth/hole opening) more than 10 with a 200-mm-diameter wafer.

Figure 1 shows the schematic view of reactor setup of 27-MHz radio frequency (RF) excited capacitively coupled plasma (CCP) source with some diagnostics. We choose this 27-MHz (with 800-kHz wafer bias) RF-CCP as a reference tool for the evaluation, because it enjoys the very high etch performance, and its uniformity of plasma in the narrow gap makes it easier to analyze the reactions in the gas phase and surface.

To evaluate the gas-phase physical parameters, probes [7], microwave interferometer [8], optical emission spectroscopy (OES) [9], and plasma absorption probe (PAP) [10] were introduced. To meas-

Table 1 Specific features of five etch systems used in the project.

Nickname	IEM	NLD	VHF	UHF	S-ECR
Cross-section					
Keywords	Narrow gap, Parallel plate, Dual frequency	Magnetic Neutral loop discharge	VHF Multi-spiral coil	UHF Spoke-wise antenna	UHF-ECR Planar antenna
RF	27.12 MHz	13.56 MHz	100 MHz	500 MHz	500, 915 MHz
Coupling	Capacitive	Inductive	Inductive	Inductive (?)	ECR (?)
Magnetic field	None	0–50 Gauss	None	None	100–400 Gauss
Te	≈4 eV	≈5 eV	≈3 eV	≈3 eV	≈2 eV
Ne	1.2×10^{11}	1.5×10^{11}	1.8×10^{11}	1.4×10^{11}	2×10^{11}
τ	6 msec	105 msec	57 msec	11 msec	17 msec
Top plate	Si, C	Quartz	Quartz	Quartz	Si, C

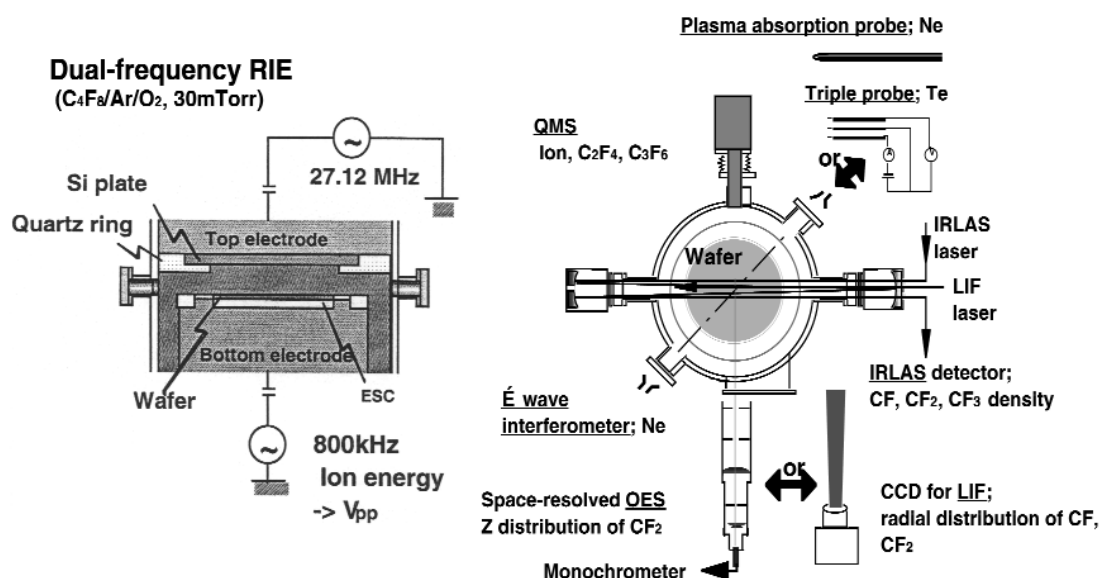


Fig. 1 Reactor setup of 27-MHz radio frequency excited RF-CCP source with diagnostics.

ure dissociated chemical species (radical), such as CF_x , infrared laser absorption spectroscopy (IR-LAS) [11,12], laser-induced fluorescence spectroscopy (LIF) [13], OES, quadruple mass spectroscopy (QMS) [14,15], and actinometry [16,17] were utilized. Furthermore, incident flux was analyzed by QMS equipped with an ion flux energy analyzer (IFEA) [18].

GENERATION OF ETCH SPECIES IN GAS PHASE AND FLUX CONTROL

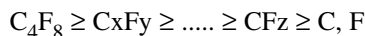
Radicals are generated in the plasma and are transported to the wafer surface, resulting in etching reaction. It is assumed that the composition of radicals determines the composition of the reactive fluorocarbon polymer formed on the etched surface, and that the etch reaction can be controlled through the composition and thickness of this polymer layer as well as the energy and flux of incident ions.

As a first step toward complete understanding of these sequential reactions, the mechanism of the radical generation in the bulk plasma should be clarified. We investigated the relation between input (external) parameters and radicals. In the following sections, radical generation mechanism and its control will be discussed.

Electron impact dissociation

Electron impact stimulates the dissociation of gas molecules in plasma. Feed gas composition, reaction at the reactor wall, also defines the composition of radical species that reach the wafer surface.

Large parent gas such as C_4F_8 obtains several electron impacts before evacuating to exhaust. Upon each electron impact, the molecule dissociates gradually into smaller radicals, i.e., multistep dissociation [19], such as,



The collision rate of C_4F_8 is given by

$$R_{\text{coll}} = ne \int_{\epsilon_{th}}^{\infty} \sigma(\epsilon)v(\epsilon)f(\epsilon)d\epsilon = ne \langle \sigma v \rangle \quad (1)$$

where n_e is the electron density, σ is dissociation collision cross-section, and v is the electron velocity. $\langle\sigma v\rangle$ means the value of σv multiplied by the normalized electron energy distribution function integrated over the threshold energy, ϵ_{th} to infinity. If we assume the electron energy distribution to be Maxwellian, $\langle\sigma v\rangle$ can be related to electron temperature T_e .

C_4F_8 suffers a multiple collisions while it travels in the plasma until it is pumped out. The total number of collisions ξ can be

$$\xi = \tau n_e \langle\sigma v\rangle \quad (2)$$

where the residence time τ is defined by the volume of plasma V , gas flow rate Q , and pressure P .

$$\tau = P V / Q \quad (3)$$

In some etch systems, such as the RF-CCP, varying the etch conditions did not show any significant change of the electron temperature. It can be assumed that the $\langle\sigma v\rangle$ is constant and the dissociation ratio of the parent gas (C_4F_8) is described by τn_e .

Figure 2 shows the radical densities and the ratio of F radical over CF_x ($x = 1-3$) radicals as a function of $\tau n_e \langle\sigma v\rangle$ in the RF-CCP reactor. Smaller radicals increased monotonously with the collision number. Relative density of F also increased linearly. Residence time τ and n_e were varied by changing Ar gas flow rate, pressure, and RF power. The total number of collisions or dissociation degree should be evaluated through a detailed study on the rate processes. However, the values of $\tau n_e \langle\sigma v\rangle$ give an idea of the dissociation process in the reactive plasma.

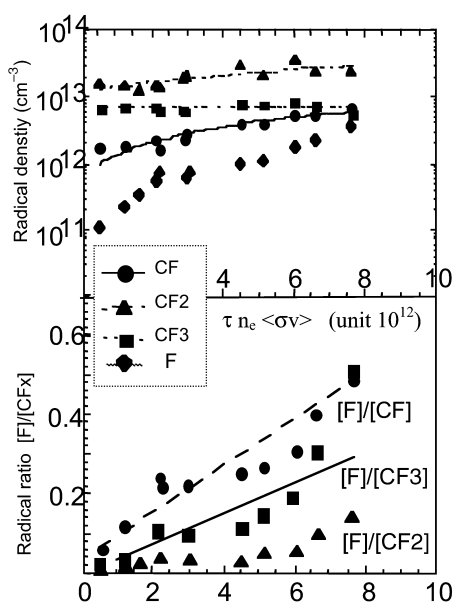
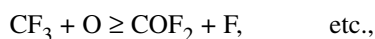
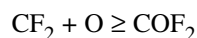
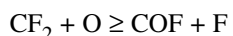
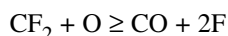
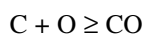


Fig. 2 Radical densities and the ratio of F radical over CF_x ($x = 1-3$) radical as a function of $\tau n_e \langle\sigma v\rangle$ in the RF-CCP reactor.

Oxygen addition

Oxygen was used to control polymer deposition on the etched surface. It is widely known that the reaction [8] can reduce the C_xF_y polymer formation both on the surface and in the bulk plasma.



This chemical reaction between C and O also has the role of cleaning the chamber surface where energetic ions are not required. As a result, the number of particles is reduced and repeatability is improved. Thus, the $C_4F_8/Ar/O_2$ based chemistry is used in the industry.

Figure 3 indicates radical density as a function of O_2 flow rate, measured in RF-CCP reactor. The CF and CF_2 radicals decreased with the increase of O_2 . On the other hand, the absolute density of F was not changed because of the reaction between the Si top electrode and the radicals [20].

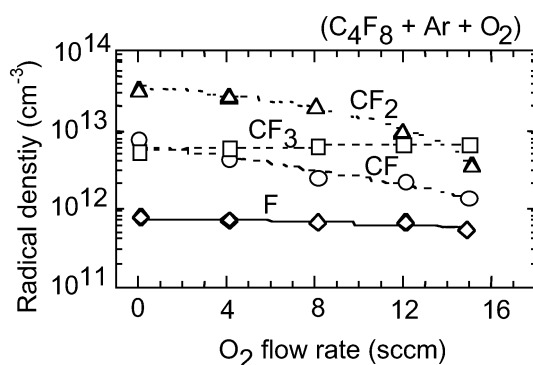


Fig. 3 Radical densities as a function of O_2 flow rate, measured in RF-CCP reactor.

Effect of plasma-wall interaction

The reaction between radicals and walls (including wafer surface) changed according to the material and temperature of the wall, incident ion energy, the surface/volume ratio of the plasma reactor, and residence time τ . It is important to note that radical density is greatly affected by the wall conditions as well as the dissociation process.

In the RF-CCP and UHF-ECR systems, the plasma was confined between the parallel plate electrodes and the RF power was supplied to top electrode for controlling the surface reaction of radicals and top plate material [21]. Figure 4 shows F densities as a function of O_2 flow rate when using Si, glassy carbon (C), or aluminium (Al) for the top electrode of RF-CCP reactor. Also, the selectivities of

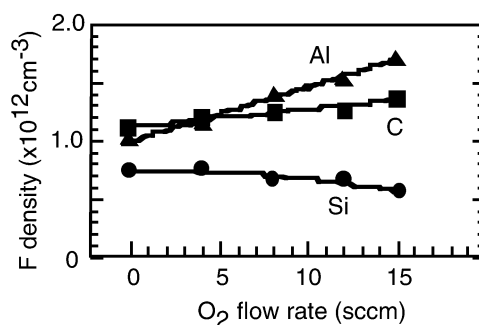


Fig. 4 F densities as a function of O_2 flow rate when using Si, glassy carbon (C), or aluminium (Al) for the top electrode of RF-CCP reactor.

SiO₂ over Si were measured with 8 sccm O₂ condition. Using an Al top plate, the selectivity was decreased by the presence of excess F radicals.

On the other hand, when we used C top plate, the decrease of selectivity was not observed in spite of the increase of F density. The C plate also releases reaction products, and an increase of OES intensities of C₂ and CO was also observed, whereas no significant change in CF, CF₂, and CF₃ densities was observed. These results indicate that the selectivity was governed by not only the absolute value of the F density or the ratio of [F]/[CF_x], but also by the other form of deposition species. It is also found that the reduction of the F density in C₄F₈/Ar plasma was caused by the decrease in CF₂ density and not by a direct reaction of F with Si when the Si plate was irradiated by energetic ions [19,22].

Flux control

The composition of radicals depends on the gas chemistry, the electron impact dissociation according to number of collisions (assumed to be $\tau n_e < \sigma v$), and interaction with the wall materials. Then, we found that a preferred (low fluorine radical content plasma) could be obtained by using a short residence time to suppress the excess dissociation of C₄F₈ and by using an ion-bombarded Si top plate to reduce the F radicals.

The next step requires clarification for how the species from the bulk plasma react on the etched surface. The SiO₂ etch rate is considered to depend on (a) composition of reactive species, (b) total flux of reactive species, (c) energy of ion, and (d) total flux of ions. Here, (a) and (b) determine the incident flux of the C-F reactive species including both ion and neutral radicals, and (c) and (d) determine the reaction energy supplied by ions accelerated by the sheath electric field on etched surface. It has been reported that etch rate is increased by increasing the ion flux, but net etch yield is not always increased [23,24]. This result suggests that optimization of (a) or (b) is necessary to obtain the maximum etch yield under each ion condition. For this reason, we controlled the amount of reactive species by varying the partial pressure of the parent gas (C₄F₈) while keeping the ion flux and ion energy constant.

In the experiments, a C₄F₈/Ar/O₂ gas mixture was used in RF-CCP. The concentration of the C₄F₈ flow rate was kept below 10 % of the total flow rate in order to keep the effect of increased electron temperature and negative ions to a minimum. Varying the partial pressure of O₂ or C₄F₈ under fixed top power conditions drastically changes the plasma density; hence, the RF powers were adjusted to obtain the same n_e of about $2 \times 10^{11} \text{ cm}^{-3}$ for each gas condition. It was also reported that the etch rate of SiO₂ depends mainly on the amount of ions at the high-energy peak in the ion flux energy distribution [23]. In this CCP system, the transit time of ions through the sheath was much shorter than the RF period, because the bias frequency was relatively low at 800 kHz. Hence, the high-energy peak of the ion flux energy distribution (IFED) could be nearly equal to the V_{pp} because incident ions are subjected to the instantaneous sheath electric field. Furthermore, we also evaluated the plasma potential (V_p) under various gas compositions while keeping n_e and V_{pp} at the same value. Under typical conditions, V_p is about 90 V. When we changed the gas composition, variation of V_p was within 50 V, a voltage much lower than the V_{pp} of 1450 V. Therefore, we assumed that the ion energy was V_{pp}.

Figure 5 shows the radical flux and the ion flux as a function of partial pressure of C₄F₈. The thermal flux of radicals (Γ_{th}) and ion flux (Γ_{ion}) were calculated by [8]

$$\Gamma_{\text{th}} = \frac{N_{\text{CFx}} \cdot n_{\text{th}}}{4} = \frac{N_{\text{CFx}}}{4} \cdot \sqrt{\frac{8kT}{\pi M_r}} \quad (4)$$

and

$$\Gamma_{\text{ion}} = n_s \cdot u_B = 0.61 \cdot n_e \cdot \sqrt{\frac{kT_e}{M_i}} \quad (5)$$

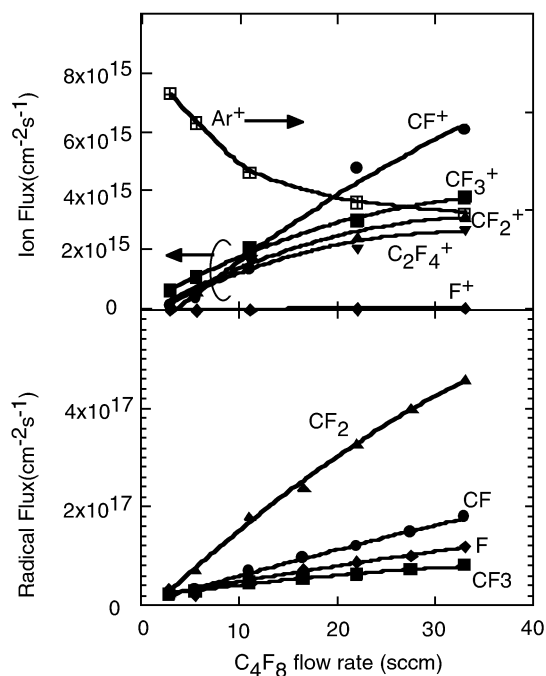


Fig. 5 Radical and ion fluxes as a function of partial pressure of C_4F_8 gas in RF-CCP.

where N_{CFx} is the CFx radical density, n_{th} is thermal velocity, k is Boltzmann constant, M_r is the mass of the radical, T is the temperature of the molecules and is assumed to be 350 K, T_e is the electron temperature of 5 eV, n_s is ion density at the sheath edge, u_B is the Bohm velocity and M_i is the mass of the ion (we used the averaged mass of all detected ions that had mass numbers from 1 to 200). As shown in Fig. 5, all of the C-F species increased monotonically with the C_4F_8 flow rate, whereas Ar decreased. The CF_2 radical was the dominant species in the bulk plasma and was on the order of $10^{17} \text{ cm}^{-2} \text{ s}^{-1}$. We estimated a total ion flux about $6 \times 10^{16} \text{ cm}^{-2} \text{ s}^{-1}$ [25.]

SURFACE REACTION MECHANISM

Figure 6 shows the etch rate of SiO_2 , Si, and Si_3N_4 as a function of C_4F_8 flow rate when $Ar/O_2 = 400/8$ sccm. The SiO_2 etch rate increased to 11 sccm and then suddenly decreased as the flow rate increased further. On the other hand, both Si and Si_3N_4 etch rates decreased when the C_4F_8 flow rate increased to 5 and 11 sccm, respectively. Then, both of the etch rates were kept constant in the very low figure.

The origin of the etch rate difference between the materials was tried to be investigated via surface analysis using X-ray photoelectron spectroscopy (XPS) [26,27] and transmission electron microscope (TEM). Figure 7 shows the CF polymer film thicknesses as a function of C_4F_8 flow rate ($Ar/O_2 = 400/8$ sccm) on each material after exposing to etching plasma. The thickness of the CF layer was estimated from the decrease of Si2p signal intensity comparing to the nonetched surface. The escape depth of the Si2p photoelectron in the CF layer was assumed to be 3.0 nm.

The thickness of the CF layer was below 1 nm before decreasing the etch rates. However, sudden increases in the thickness were observed as increase of the C_4F_8 flow rate. They correspond to the drops in the etch rate of each material. It is considered that the excess CF layer worked as an inhibitor for the etch reaction.

Figure 8 shows that a TEM image at the bottom of the contact hole etched under the condition of $C_4F_8/Ar/O_2 = 11/400/8$ sccm. Ru was deposited at room temperature after the etching. On the Si sub-

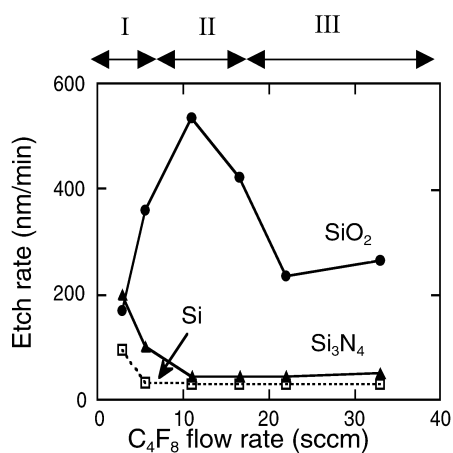


Fig. 6 Etch rates of SiO_2 , Si, and Si_3N_4 as a function of C_4F_8 flow rate, $Ar/O_2 = 400/8$ sccm.

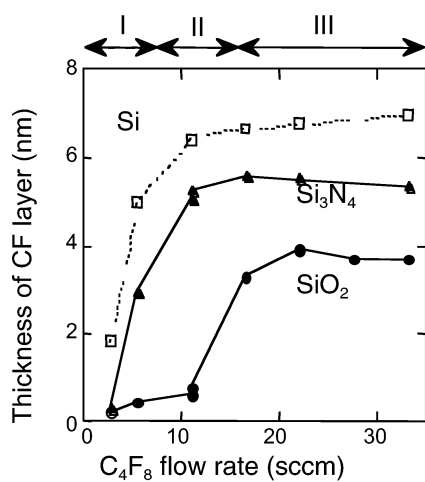


Fig. 7 CF polymer film thicknesses as a function of C_4F_8 flow rate ($Ar/O_2 = 400/8$ sccm) on each material after exposing to RF-CCP plasma.

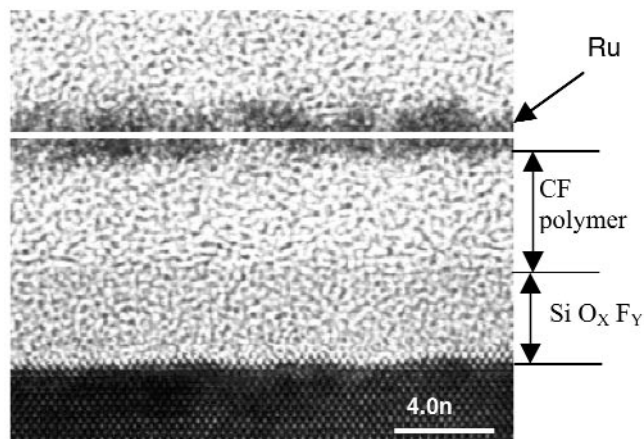


Fig. 8 TEM image at bottom of contact hole etched by RF-CCP, $C_4F_8/Ar/O_2 = 11/400/8$ sccm.

strate, two layers were observed. We think the top layer was CF and the second layer was SiF_xO_y. The TEM image agreed well with the XPS results.

To consider a limiting process of the etch rates, we divided the etch conditions to three regions in Figs. 6 and 8. Region I is under-flux (thin polymer) condition, region II is the highly selective condition, and region III is over-flux condition. In region II, there is a very large difference in the CF layer thickness on the SiO₂ and other films. This must be the main origin of the selectivity change as the radical flux changes.

Basic model for SiO₂ etch reaction

We tried to establish a simple model to explain all of the etching characteristics of each material based on the surface analysis results [28]. First, in the under-flux condition (region I in Fig. 6) where the surface CF polymer was less than 1 nm on SiO₂, we examined the various data and found out that the total number of incident F atoms, $\Gamma_{F\text{-total}}$ can express well the etch rate change as shown in Fig. 9. $\Gamma_{F\text{-total}}$ was calculated from the net C-F fluxes, Γ_{net} that was given by the Milne boundary condition [29].

$$\Gamma_{\text{net}} = \frac{2s}{2-s} \cdot \Gamma_{\text{th}} \quad (6)$$

where Γ_{th} is thermal flux of the radicals described in eq 4, s is the surface reaction probability. The net flux is the ratio of the number of species that actually react with the etched material to the total number of incident species. So we calculate the net radical flux of CF, CF₂ and CF₃, respectively using the reported values of s , 5×10^{-4} , 6×10^{-5} , and 2×10^{-3} [30]. The calculated values of net radical flux were on the order of $10^{14} \text{ cm}^{-2}\text{s}^{-1}$. The CF_x ion fluxes were estimated to be the order of $10^{15}\text{--}10^{16} \text{ cm}^{-2}\text{s}^{-1}$.

On the other hand, typical SiO₂ etch rate by these flux condition was 500 nm/min and the out-flux of Si from the surface was about $4 \times 10^{16} \text{ cm}^{-2}\text{s}^{-1}$. A comparison of these orders of fluxes tells that the amount of net radical flux estimated here is too small as a dominant species that determines the SiO₂ etch rate. We speculated that we had underestimated the net radical flux that was determined mostly by s . The reported s values were taken on a surface exposed to a low-density plasma, and the ion bombardment energy was too small. In our experiment, the surface was bombarded by ions with the energy more than 1 keV and large flux as $10^{16} \text{ cm}^{-2}\text{s}^{-1}$. It has been reported that the adsorption of CF₂ radicals increases by a surface activation caused by ion bombardment [31].

Based on the discussion above, we estimated the surface reaction probability s as using many different sets of s (varying s from 0.01 to 1 for each radical species), and determined the appropriate cor-

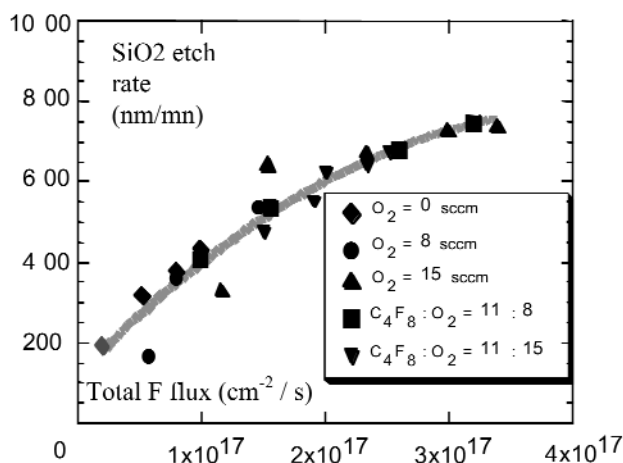


Fig. 9 SiO₂ etch rate in various conditions when surface CF polymer was less than 1 nm (region I in Fig. 6) as a function of $\Gamma_{F\text{-total}}$.

respondence for making observations. We found that the SiO_2 etch rate could be expressed by the number of incident total F atoms $\Gamma_{\text{F-total}}$, when assuming $s = 0.1$.

It is not concluded which kind of species are the dominant etch species because we cannot control the amount of species in the ions and radicals independently in the plasma reactor. We observed that the incident number of F in the ion fluxes (F^+ , CF^+ , CF_2^+ , CF_3^+ , C_2F_4^+ , and C_3F_5^+) also increased when increasing that in the radical flux. The real values of s are still unclear, and further research on these constants at the realistic etching surface should be conducted.

Etch rates under $V_{\text{pp}} = 1450, 1200, 900,$ and 600 V are plotted as a function of $\Gamma_{\text{F-total}}$ assuming constant $s = 0.1$, as shown in Fig. 10. In the lower energy condition, the etch rates are relatively low with the same $\Gamma_{\text{F-total}}$. The s is a function of the ion energy, because it must depend on the density of surface sites (dangling bonds on the reactive surface layer, which is generated by the ion bombardment). Then, we reestimated the s value as shown in Fig. 10b, with which all data in Fig. 10a could be replotted in a same curve in Fig. 10c. These fitted s values must have errors, however, the trend over the ion energy is consistent with the data estimated from beam experiments [32]. It is concluded that $\Gamma_{\text{F-total}}$, that is a function of s , increases with the ion energy, and the etch rate is a function of both F containing species fluxes and the reaction probability, s that depends on the ion energy supplied to the reaction layer.

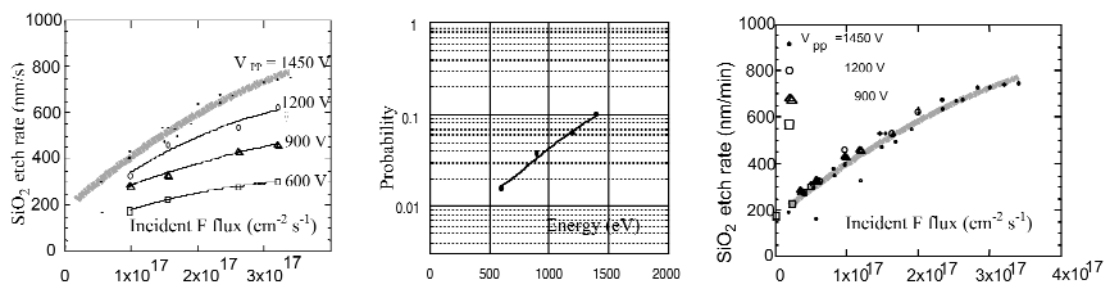


Fig. 10 (a) Etch rates under $V_{\text{pp}} = 1450, 1200, 900,$ and 600 V as a function of $\Gamma_{\text{F-total}}$ assuming constant $s = 0.1$; (b) re-estimated s value for ion energy; (c) replotted etch rates in (a) using s estimated in (b).

Etch rate model with CF polymer

Figure 11 shows the etch rate as a function of $\Gamma_{\text{F-total}}$ ($s = 0.1$) for various CF layer thickness T_{CF} . CF layer thickness was changed by O_2 flow rate. The etch rate becomes lower for the thicker CF film. This indicates that the s should be changed for the thicker CF polymer condition. It may be because the incident ion energy decreased while ions passed through the thick CF polymer layer. It has been reported that the projection range of ions can be calculated roughly using the Ziegler–Biersack–Littmark (ZBL) model [33,34]. For example, the projection range of 500 eV Ar^+ to Si is estimated about 5 nm. It means the most of ion energy is lost within a few nanometers of the top surface.

The ion energy that reaches the reaction layer beneath the CF polymer must be changed according to the T_{CF} . Therefore, we have to take into account the energy loss ΔV and use the net energy V_{net} to determine the surface reaction probability s .

$$V_{\text{net}} = V_{\text{pp}} - \Delta V(T_{\text{CF}}) \quad (7)$$

Comparing Fig. 10a and Fig. 11a, the plots for a 4-nm-thick polymer corresponded to the plots of $V_{\text{pp}} = 600$ V. The energy loss ΔV was estimated similarly for different conditions as shown in Fig. 11b. It is clearly shown that the ΔV increases monotonically with T_{CF} . Using reestimated s values for thick-polymer conditions, $\Gamma_{\text{F-total}}$ values were calculated again. Then, all SiO_2 etch rates were plotted in the

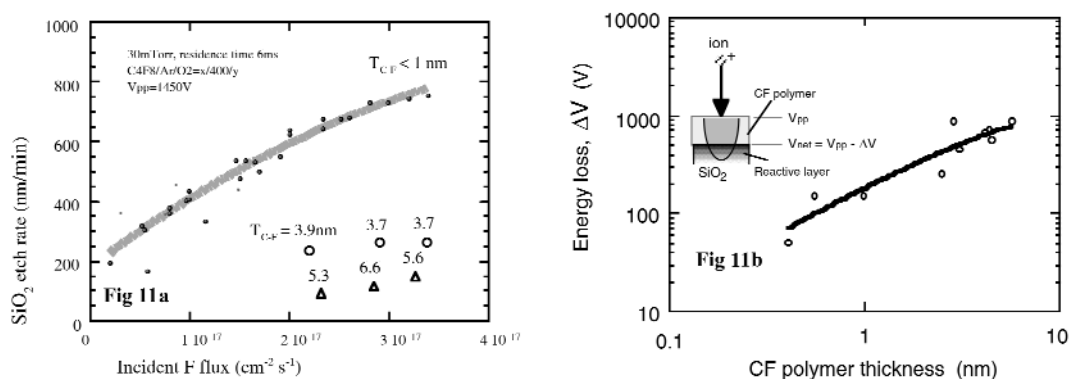


Fig. 11 (a) Etch rate as a function of $\Gamma_{F\text{-total}}$ ($s = 0.1$) for various CF layer thickness, T_{CF} ; (b) energy loss ΔV as a function of CF layer thickness T_{CF} .

same curve for $T_{CF} < 1$ nm in Fig. 11a. Now, the etch rates for any conditions are well expressed by the $\Gamma_{F\text{-total}}$.

CF polymer thickness

In the experiments, we used the XPS to measure the CF polymer thicknesses. To establish a model to predict the etch rate only using the data of ion current, energy, and species density compositions that may be simulated from input parameters (recipe) of etch systems, it is very important to know how the thickness of CF polymer is determined. We estimated the polymer thickness by the balance of C atoms,

$$\rho \frac{dT_{CF}}{dt} = \Gamma_{C\text{-total}} - L_{ion} - L_O - L_F = 0 \quad (8)$$

where ρ is the density of CF polymer, $\Gamma_{C\text{-total}}$ is the total number of incident C atoms in the CF_x fluxes, L_{ion} , L_O , L_F are the rates of carbon removal (loss term) by the reaction with ion, oxygen, and fluorine, respectively. L_{ion} is a function of the ion energy, ion flux, and sputtering yield of the polymer that depends on composition, such as the C/F ratio. Reaction with oxygen is most important because carbon easily reacts with oxygen. Besides the incident flux oxygen from the gas phase ($L_{O\text{-plasma}}$), it is supplied from the SiO₂ as an etch product ($L_{O\text{-sub}}$).

Fluorocarbon (CF) film formation from the beginning of the etching process was observed until the film reaches a steady state at a specific thickness. Using *in situ* time-resolved infrared spectroscopy with attenuated total reflection (ATR), we measured spectra every 2 s and observed CF film formation during plasma etching of SiO₂/Si film on a prism wafer, i.e., crystalline germanium substrate [35].

The observed spectra were shown in Fig. 12a. A band at around 1200–1400 cm⁻¹ caused by CF bonds overlapped with a trough at below 1300 cm⁻¹ caused by Si–O bonds. Each component of the spectra in the series was deconvoluted to obtain time-resolved intensity profiles in Fig. 12b. It is found that while the oxide was being etched, the Si–O peak decreased and the CF film grew soon and its thickness reached a steady state.

Furthermore, the CF signal increased again and gradually reached a constant value. The reason that the CF layer grew upon the exposure of Si after SiO₂ was etched off is that the out-flux from SiO₂ stops and the loss term $L_O (= L_{O\text{-plasma}} + L_{O\text{-sub}})$ decreases in the CF-film balance, eq 8. The loss term due to the out-flux differs in each materials. Their difference causes the different CF layer thickness between the materials and originates the selectivity.

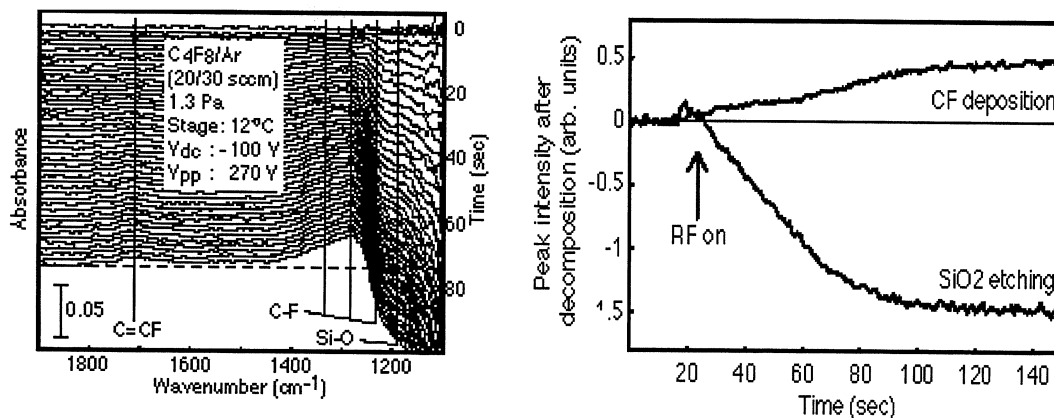


Fig. 12 (a) IR-ATR spectra during plasma etching of SiO_2/Si film; (b) deconvoluted spectra for CF film formation and SiO_2 etching.

The CF layer soon reaches a constant thickness after the change of condition. This means that we need a loss term that increases according to the CF thickness. It is probably the loss term by ion bombardment (L_{ion}) because the loss of ion energy should increase for a thicker CF film.

SIMULATION OF ETCH RATE

We developed a simple program [36] that calculates the etch rate for SiO_2 , Si, Si_3N_4 , and Si-containing organic materials, based on the surface reaction mechanism discussed above. As the input data for the calculation, we used information of material and internal parameters of reactive plasma. The former is an atomic composition and the density of the material to be etched. The latter is radical composition, radical density, ion energy that gives incident fluxes for ions and radicals. It is possible to obtain these parameters using a plasma simulator that calculates these internal parameters from the external parameters, i.e., reactor configuration, process recipe, data obtained from simple monitoring systems such as the OES and probes. The calculating steps will be repeated until the etch rate converging because the etch rate gives the out-flux and changes T_{CF} .

Figure 13 shows examples of the calculation results for SiO_2 etch rate and the selectivity over Si when changing the C_4F_8 and O_2 flow rates individually. This program succeeded to predict the absolute

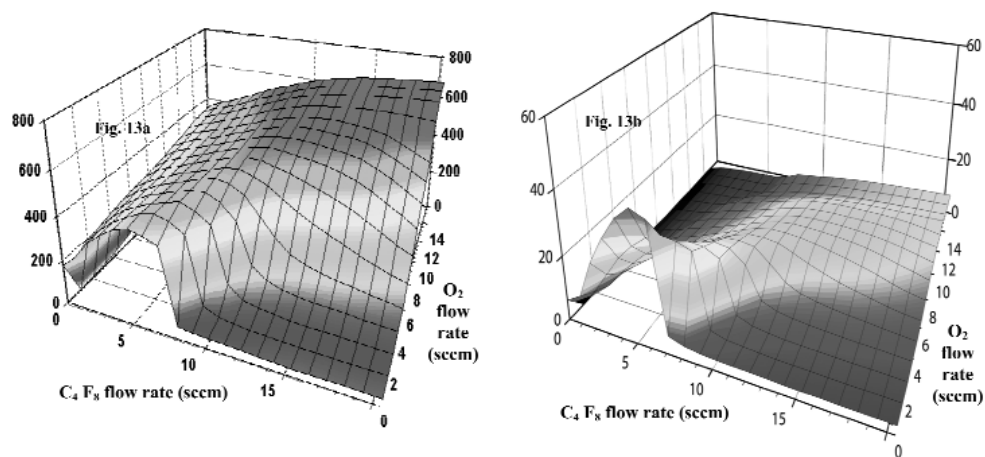


Fig. 13 Example of calculation results for SiO_2 etch rate and selectivity over Si when changing C_4F_8 and O_2 flow rates individually.

value of the etch rates. It is very useful to know how each parameter affects the etch rate and the selectivity including their process margin. It will help us to construct a specific etch recipe fast.

PHENOMENA IN DEEP HOLE

The basic etch mechanism was investigated with the intensive research on the gas phase, and the surface reactions occurred in a reactive fluorocarbon plasma used for real wafer processing. However, etch results in a small hole are often different from the results in a large area. The phenomena in deep and high-aspect-ratio holes [37] are not well understood yet. Therefore, we developed a real-contact-hole-sized (0.2–0.3 μm diameter) micro-capillary plate (MCP) for measuring the incident fluxes passed through the deep holes [38]. Comparing the data with that derived from an ion-transportation simulation could reveal the amount of energy and current loss when ions were traveling in a deep hole.

A micro-machining technology was used to fabricate MCPs in a Si wafer. The MCP had an electrostatic virtual bottom structure that designed to realize a charge build-up potential around the end of the hole as if the bottom exists. The MCP was placed on the electrode of NLD etcher. The ions passed through the MCP were detected using the ion flux energy analyzer (IFED) set under the electrode. The transmittance factor of the MCP is about 4 %.

Figure 14 shows typical results obtained using MCP at various aspect ratios. $A/R = 0$ means that the ion flux was measured directly from a 0.2- μm -diameter orifice without the MCP. The ion flux shown in Fig. 14 was not normalized between the data with and without the MCP. It was found that (1) the energy shift of the high energy peaks from $A/R = 0$ is as small as 20 V; (2) the low-energy peaks for IFED via MCP disappeared; and (3) decrease of the ion current after passing through the MCP was less than 20 % of the current without the MCP.

When using large-size CP (10–50 μm diameter, ~ 400 μm thick), a large shift of the high-energy peak and decrease of ion flux up to 40 % were observed. This energy shift and ion flux loss corresponds well to the calculation assuming no leakage current between the surface and bottom region of the CP.

Consequently, the flux and energy of ions passing through the MCP holes is not modified much due to some conduction paths. In the actual contact hole etching, the bottom charge build-up potential

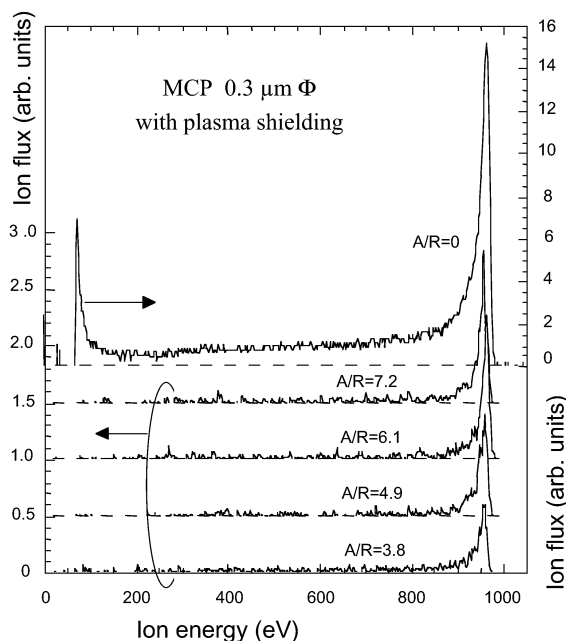


Fig. 14 Ion flux energy distribution (IFED) measured through MCP at various aspect ratios.

must increase to only several tens of volts. Specific phenomena for high-aspect-hole etching, such as the micro-loading effect and etch stop, should be considered from the viewpoint of the neutral radical transfer in the hole.

SUMMARY

ASET Plasma Laboratory had conducted a systematic research on the SiO₂ etching using fluorocarbon (CF) plasma. The 5-year program finished in March 2001, revealed basic etch mechanisms from the etch species generation to the reaction in a deep hole. The number of electron collisions to fluorocarbon gas molecule is proposed as an important parameter to control the gas dissociation and etch species flux to the surface. An etch reaction model was proposed and successfully predicted the etch rates of Si-containing materials. Requirements for the development of next-generation etch tools were discussed.

ACKNOWLEDGMENTS

The author thanks Profs. T. Goto (Nagoya Univ.), K. Tachibana (Kyoto Univ.), H. Sugai (Nagoya Univ.), T. Makabe (Keio Univ.), Y. Horiike (Tokyo Univ.), and K. Muraoka (Kyusyu Univ.) for their subcontract research in the project. This work was performed under the management of ASET in an R&D program of the Ministry of Economy, Trade, and Industry (METI) supported by the New Energy and Industrial Technology Development Organization (NEDO).

REFERENCES

1. M. Inoue, A. Ishitani, A. Samukawa, M. Sekine. *J. Vac. Sci. Technol. A* **16**, 341 (1998).
2. T. Tatsumi, H. Hayashi, S. Morishita, S. Noda, M. Okigawa, N. Itabashi, Y. Hikosaka, M. Inoue. *Jpn. J. Appl. Phys.* **37**, 2394 (1998).
3. T. Okumura and I. Nakayama. *Rev. Sci. Instrum.* **66**, 5262 (1995).
4. K. Yokogawa, N. Itabashi, N. Negishi, K. Suzuki, S. Tachi. *Proc. of the 191st Meeting of Electrochemical Society*, Montreal, G2 (1997).
5. S. Samukawa, Y. Nakagawa, T. Tsukada, H. Ueyama, K. Shinohara. *Appl. Phys. Lett.* **67**, 1414 (1995).
6. T. Uchida. *Jpn. J. Appl. Phys.* **33**, L43 (1994).
7. I. Langmuir and H. M. Mott-Smith. *Phys. Rev.* **28**, 727 (1926).
8. M. A. Lieberman and A. J. Lichtenberg. *Principles of Plasma Discharges and Materials Processing*, Wiley, New York (1995).
9. S. Noda, M. Okigawa, N. Itabashi, Y. Hikosaka, K. Kinoshita, T. Tatsumi, H. Nakagawa, M. Inoue. *Proc. 19th Symp. Dry Process*, p. 327 (1998).
10. H. Kokura, K. Nakamura, I. Ghanashev, H. Sugai. *Jpn. J. Appl. Phys.* **38**, 5262 (1999).
11. M. Magane, N. Itabashi, N. Nishiwaki, T. Goto, C. Yamada, E. Hirota. *Jpn. J. Appl. Phys.* **29**, L829 (1990).
12. K. Maruyama, A. Sakaki, T. Goto. *J. Phys. D* **26**, 199 (1993).
13. J. P. Booth, G. Hangcock, N. D. Perry, M. J. Toogood. *J. Appl. Phys.* **66**, 5251 (1989).
14. H. Sugai and H. Toyoda. *J. Vac. Sci. Technol. A* **10**, 1193 (1992).
15. H. Toyoda, M. Ito, H. Sugai. *Jpn. J. Appl. Phys.* **36**, 3730 (1997).
16. J. W. Coburn and M. Chen. *J. Appl. Phys.* **51**, 3134 (1980).
17. Y. Kawai, K. Sasaki, K. Kadota. *Jpn. J. Appl. Phys.* **36**, L1261 (1997).
18. Y. Hikosaka, H. Hayashi, M. Sekine, H. Tsuboi, M. Endo, N. Mizutani. *Jpn. J. Appl. Phys.* **38**, 4465 (1999).

19. H. Hayashi, S. Morishita, T. Tatsumi, Y. Hikosaka, H. Nakagawa, S. Kobayashi, M. Inoue, T. Hoshino. *J. Vac. Sci. Technol.* **17**, 2557 (1999).
20. T. Tatsumi, H. Hayashi, S. Morishita, S. Noda, M. Okigawa, N. Itabashi, Y. Hikosaka, M. Inoue. *Jpn. J. Appl. Phys.* **37**, 2394 (1998).
21. S. Morishita, H. Hayashi, T. Tatsumi, Y. Hikosaka, S. Noda, M. Okigawa, M. Inoue. *Jpn. J. Appl. Phys.* **37**, 6899 (1998).
22. H. Hayashi, M. Okigawa, S. Morishita, M. Sekine. *J. Vac. Sci. Technol. A* **17**, 2517 (1999).
23. Y. Hikosaka, H. Hayashi, M. Sekine, H. Tsuboi, M. Endo, N. Mizutani. *Jpn. J. Appl. Phys.* **38**, 4465 (1999).
24. N. Mizutani and T. Hayashi. *Jpn. J. Appl. Phys.* **36**, L1470 (1997).
25. T. Tatsumi, Y. Hikosaka, S. Morishita, M. Matsui, M. Sekine. *J. Vac. Sci. Technol. A* **17**, 1562 (1999).
26. G. S. Oehrlein, Y. Zhang, D. Vender, M. Havelag. *J. Vac. Sci. Technol. A* **12**, 323 (1994).
27. M. Matsui, T. Tatsumi, M. Sekine. *J. Vac. Sci. Technol. A* **19**, 2089 (2001).
28. T. Tatsumi, M. Matsui, M. Okigawa, M. Sekine. *J. Vac. Sci. Technol. A* **18**, 1897 (2000).
29. Y. Hikosaka and H. Sugai. *Jpn. J. Appl. Phys., Part 1* **32**, 3040 (1993).
30. K. Miyata, M. Hori, T. Goto. *Jpn. J. Appl. Phys., Part 1* **36**, 5334 (1997).
31. K. Takahashi, M. Hori, M. Inayoshi, T. Goto. *Jpn. J. Appl. Phys., Part 1* **35**, 3635 (1996).
32. D. C. Gray. Ph.D. thesis, MIT, Dept of Chemical Engineering, 1992.
33. J. F. Ziegler, J. P. Biersack, W. Littmark. *The Stopping and Ranges of Ions in Matter*, Vol. 4, Pergamon, New York (1985).
34. M. Matsui, F. Uchida, T. Tokunaga, H. Enomoto, T. Umezawa. *Jpn. J. Appl. Phys., Part 1* **38**, 2124 (1999).
35. K. Ishikawa and M. Sekine. *Jpn. J. Appl.* **39**, 6990 (2000).
36. <http://www.aset.or.jp/plasma>
37. K. Kurihara and M. Sekine. *Plasma Sources Sci. Technol.* **5**, 12 (1996).
38. S. Noda, N. Ozawa, T. Kinoshita, H. Tsuboi, K. Kawashima, Y. Hikosaka, K. Kinoshita, M. Sekine. *Thin Solid Films* **374**, 181 (2000).